

e-mail: Michael.Feser@sunysb.edu

Scanning Transmission X-ray Microscopy With a Segmented Detector

M. Feser¹, C. Jacobsen¹, P. Rehak² and G. DeGeronimo²

¹ *Department of Physics and Astronomy, SUNY Stony Brook, USA*

² *Instrumentation Division, Brookhaven National Laboratory, USA*

Abstract

A segmented silicon detector has been developed for the Stony Brook soft x-ray scanning transmission x-ray microscope. The detector combines good detective quantum efficiency (90% at 520 eV) and low noise (≈ 5 photons/channel/integration at 520 eV) with the ability of having up to 10 independent sensitive regions that are matched to the microscope geometry. In addition to the usual bright field images, differential phase contrast images and dark field images are recorded simultaneously in one scan. A Fourier filtering method has been employed to recover an estimate of the sample absorption and phase shift from the partially coherent images collected on the detector segments. A reconstruction of a Germanium test pattern exhibits good agreement between the predictions from the tabulated x-ray optical constants and the experiment.

1 INTRODUCTION

In scanning transmission x-ray microscopy (STXM) commonly a large area counting detector is employed for incoherent imaging. This is well suited for quantitative X-ray absorption measurements, but is completely insensitive to the phase shifts introduced by the specimen. A detector with some degree of spatial resolution is capable of also recovering information about the phase shift of the specimen. Another limitation of counting detectors is the maximum count rate they can detect and nonlinearity if run close to this limit. In Sec. 2 we describe the novel integrating silicon detector with segmentation, which addresses the needs for higher count rate capability and spatially resolved photon detection.

Phase contrast is important for samples with low absorption contrast, but appreciable phase contrast, like low-Z specimens at higher (> 1 keV) photon energies. For lower photon energies it can lower the radiation dose by using the phase shift and not the absorption as the contrast mechanism [10].

The theory of differential phase contrast in STXM with the use of a split and first moment detector was first explored by Palmer and Morrison [9]. If the full spatial distribution of x-rays in the detector plane is recorded with a pixel detector (CCD) for each probe position on the specimen, the specimen phase can be recovered by Wigner distribution deconvolution (WDC). Additionally the properties of the imaging system can be recovered from the highly redundant dataset, which has been demonstrated in STXM by Chapman [1]. Although it is desirable to sample the intensity distribution in the detector plane finely with a pixel detector, practical considerations like the amount of data generated and the slow speed of the detector currently discourage this approach. New developments in the use of CCD detectors in STXM [8] are very promising, but still require long exposure times and require offline processing. We are reviewing the image formation process in STXM with a segmented detector in Sec. 3

in reference to the particular detector geometry we used.

For a more general choice of detector segments, images formed by taking differences from opposing segments become difficult to interpret, because they no longer represent well a measure of the phase gradient. In Sec. 4 we present a Fourier filtering technique originally developed for the scanning electron microscope by Landauer, McCallum and Rodenburg [6], which uses the contrast transfer functions calculated in Sec. 3 to reconstruct an estimate of the specimen absorption and phase.

Experimental results obtained on the Stony Brook scanning transmission x-ray microscope at the NSLS are presented in Sec. 5. We have obtained a high resolution complex reconstruction of a Germanium test pattern, which agrees quantitatively very well with the tabulated optical constants [4] for Germanium.

2 INTEGRATING SILICON DETECTOR WITH SEGMENTATION

The integrating Silicon detector with segmentation has two main components: the silicon chip and the low noise analog readout electronics.

The chip is fabricated out of 300 μm thick high resistivity n-type silicon. A planar technology adapted for detector production [5] is employed to pattern rectifying p/n junctions with separate current readout on the front side of the chip. The p-type implant is very shallow to yield excellent quantum efficiency for soft x-rays ($\approx 80\%$ for 280 eV, $\geq 90\%$ for 520 eV). The back side has an ohmic contact (without patterning) for the application of a bias voltage. If the chip is illuminated from the back side the quantum efficiency is comparable to the front side, which was verified experimentally. The chip is used in the back side illumination configuration in which the positive holes generated by the x-rays are drifted through the depleted silicon substrate to the patterned p-side. The necessary higher backside bias (≈ 90 V for back side, ≈ 1.5 V for front side illumination) is tolerated in favor for the superior radiation damage resistance of the back side contact. Fig. 1b shows the patterning of the detector chip. The inner three segments and the four quadrant segments are being used for phase contrast measurements. The large outermost segment is detecting x-rays scattered out of the illumination pupil, which corresponds to a darkfield detector. The segmentation is not optimal for the work presented here due to the historical segmentation scheme, but an improved segmentation design is in the production process.

A simplified schematic of one channel (ten total) of the charge integrating electronics is shown in Fig. 1a. The corresponding detector segment is represented as a diode at the left side. At the beginning of each integration period an FET switch (S1) resets the feedback capacitor of the preamplifier (PA). The output voltage of the PA is stored on a capacitor on the positive input of the instrumentation amplifier (IA) by closing the switch S2 for a short time bringing the output of the IA to zero. When S2 is opened, the output of the IA rises linearly with the charge that is collected on the feedback capacitor of the PA. A sample and hold circuit (S3) stores the output value at the end of the integration cycle for readout. The switches S1 through S3 are controlled externally allowing a variable clock rate.

With an integration time ranging from 1 to 3 ms we have measured the noise of the complete system to be ≈ 5 photons/channel/integration (520 eV photons). In practice this noise is much smaller than the uncertainties introduced by photon statistics (photon shot noise) for bright field measurements making it competitive with counting detectors. In the current configuration the maximum number of photons that can be detected in one channel is 1×10^4 without a limitation on the photon flux, giving the integrating detector a big advantage over counting detectors for high photon flux experiments.

A more comprehensive description of the detector can be found in the Ph.D. dissertation of Feser [2] and in a paper that is under preparation [3].

3 IMAGE FORMATION WITH A SEGMENTED DETECTOR

Fig. 2 shows the arrangement of the zone plate (ZP), the specimen and the detector in STXM. It is convenient to describe the coordinates in the ZP and detector plane in terms of spatial frequencies \vec{f} ,

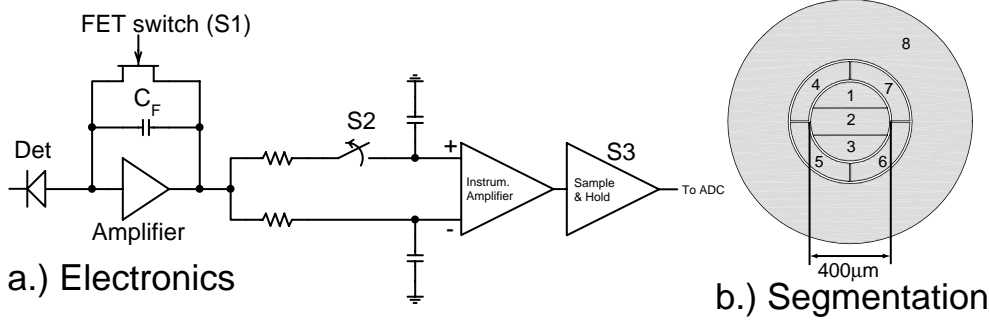


Fig. 1. Simplified schematic of the integrating electronics (a). Layout of the detector segments (b).

which are reciprocal to the real space coordinates \vec{r} in the specimen plane. We assume that the ZP acts like a perfect thin lens and that it is illuminated by a monochromatic plane wave. The illuminating wave field, limited aperture and apodization of the ZP is described by the pupil (or aperture) function $P(\vec{f})$. In the simplest case this function is a constant where the zones of the ZP are and zero otherwise. The specimen is represented by a multiplicative complex function $h(\vec{r})$, and its frequency spectrum by $H(\vec{f})$. The scanning process is included as a vector \vec{r}_0 describing the displacement of the probe on the specimen. We are interested in the images $s_k(\vec{r}_0)$ which are formed on a detector with a detector response function $R_k(\vec{f})$. $R_k(\vec{f})$ is real valued and constant on a detector segment k and zero otherwise. It can be shown [2] that the Fourier transform of the image $s_k(\vec{r}_0)$ formed by detector segment k is given by:

$$S_k(\vec{f}_0) = \int R_k(\vec{f}) \left\{ \left(P(\vec{f}) P^*(\vec{f} - \vec{f}_0) \right) \otimes_{\vec{f}} \left(H(\vec{f}) H^*(\vec{f} + \vec{f}_0) \right) \right\} d\vec{f} \quad (3.1)$$

The symbol $\otimes_{\vec{f}}$ denotes a convolution in respect to the variable \vec{f} . If the specimen is weak, the specimen function can be written $h(\vec{r}) \approx 1 - a(\vec{r}) - i\phi(\vec{r})$, where $a(\vec{r})$ and $\phi(\vec{r})$ are real valued functions. The Fourier transform then takes the Form $H(\vec{f}) \approx \delta(\vec{f}) - A(\vec{f}) - i\Phi(\vec{f})$. If we neglect the terms not picked out by the delta function, Eq. 3.1 is simplified to:

$$S_{\vec{f}} = \delta(\vec{f}) - A(\vec{f}) T_a^k(\vec{f}) - i\Phi(\vec{f}) T_\phi^k(\vec{f}), \quad (3.2)$$

where we have introduced the amplitude contrast (AC) and phase contrast (PC) transfer functions:

$$T_a^k(\vec{f}), T_\phi^k(\vec{f}) = C_k(0, 1, \vec{f}) \pm C_k(-1, 0, \vec{f}) \quad (3.3)$$

and the integral

$$C_k(m, n, \vec{f}) = \int P(\vec{f}_1 - m\vec{f}) P^*(\vec{f}_1 - n\vec{f}) R_k(\vec{f}_1) d\vec{f}_1. \quad (3.4)$$

In this approximation the resulting image for a detector segment k is a Fourier filtered version of the specimen function. The imaging process therefore is described completely by the Fourier filters (transfer functions) independently of the specimen. If the pupil function ($P(\vec{f})$) is real valued (i.e. no defocus or deviation from plane wave), the contrast transfer functions are also real valued, which we assume in the following. Figs. 3cd depict the calculated AC and PC transfer functions for one of the detector segments (cf. Fig. 3b) of the integrating silicon detector with segmentation (cf. Sec. 2). The AC transfer function generally has even symmetry while it is odd for PC. If the pupil function (cf. Fig. 3a) is rotationally symmetric, the AC transfer functions of opposing detector segments are identical, but the PC transfer functions change sign. The images formed by adding the signal of opposing detector

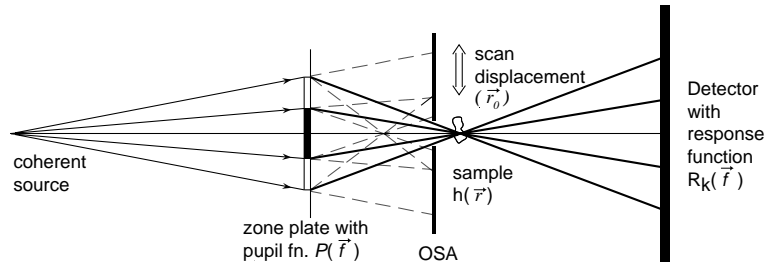


Fig. 2. Image formation in STXM.

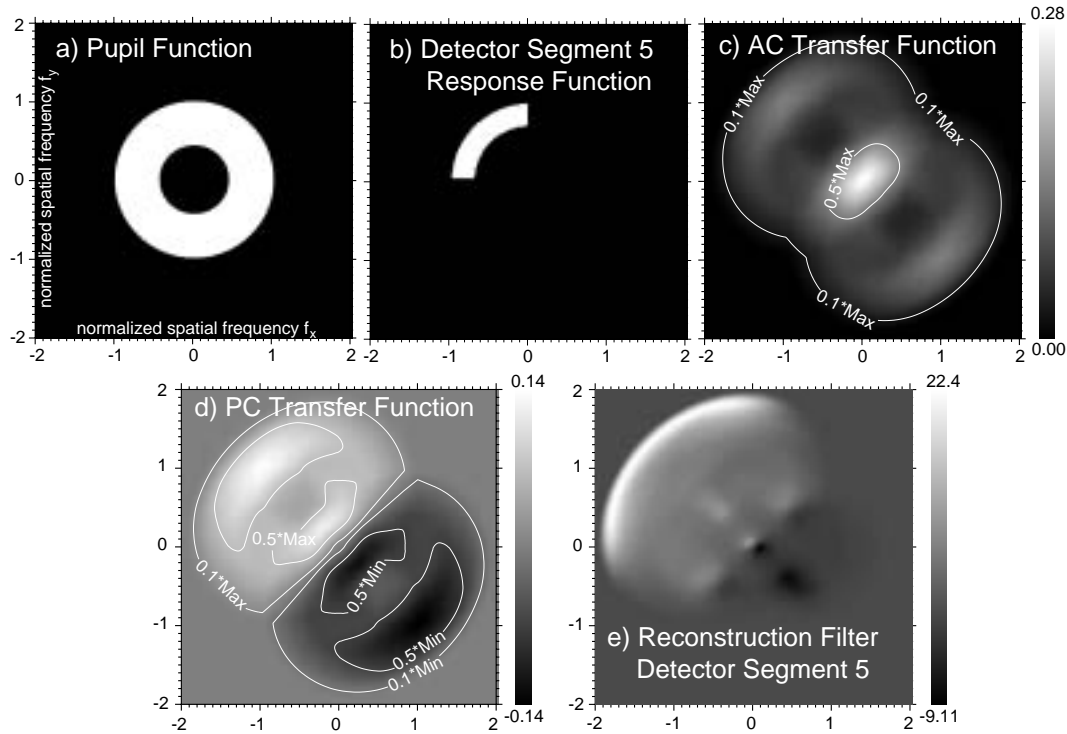


Fig. 3. Example of (c) calculated amplitude contrast (AC) and (d) phase contrast (PC) transfer functions from (a) the pupil function and (b) the detector response function of one segment. A resulting reconstruction filter is shown in (e).

segments then only is exhibiting AC, while the difference images only exhibit PC. Since the behavior of the AC and PC transfer functions can be quite complex for a specific choice of detector segmentation, images formed by taking sums and differences can be difficult to interpret.

4 FOURIER FILTER RECONSTRUCTION OF COMPLEX SPECIMEN FUNCTION

The inverse problem to the image formation, namely how to recover the complex specimen function from images obtained from the different detector segments, has been addressed in the electron microscopy community [6, 7]. The best estimate of the Fourier representation of the specimen function is

found to also be a Fourier filter:

$$\hat{H}(\vec{f}) = \sum_k W_k(\vec{f}) S_k(\vec{f}), \quad (4.1)$$

with filter functions $W_k(\vec{f})$ given by:

$$W_k(\vec{f}) = \frac{T_a^{(k)*}(\vec{f})}{\sum_l |T_a^l(\vec{f})|^2 + \beta_a(\vec{f})} + \frac{T_\phi^{(k)*}(\vec{f})}{\sum_l |T_\phi^l(\vec{f})|^2 + \beta_\phi(\vec{f})}. \quad (4.2)$$

The noise parameters $\beta_{a,\phi}(\vec{f})$ generally depend on Fourier spectrum of the sample like in a Wiener filter, but in practice they can be set to a suitable constant. Since the filter functions in Eq. 4.1 only contain AC and PC contrast transfer functions for a constant β , they can be computed in advance and don't change. Fig. 3e shows an example of a computed Fourier filter for one detector segment.

5 EXPERIMENTAL RESULTS

We have used this reconstruction method for images taken of a Germanium test pattern (cf. Fig. 4) with the segmented detector. At the x-ray imaging energy of 520 eV Germanium is quite absorbing, but the ratio of β (the amplitude component of n) to δ (phase shift) is relatively small, $\beta/\delta = 0.346$ [4]. The image of the imaginary (phase) part of the specimen shows significantly higher contrast than the real (amplitude) part. On the phase images small patches of left over organic resist, which also have a stronger phase shift than absorption, are resolved in detail. The images also illustrate that fluctuations in the intensity of the x-ray beam only transfer to the amplitude image and are completely absent in the phase image. A quantitative analysis of the reconstruction shows that for this high spatial frequency object the measured ratio of β/δ for the Germanium structures varies from 0.3 to 0.4 over the whole field of view. This is in excellent agreement with the tabulated value of 0.346.

6 CONCLUSION

A novel segmented detector with 10 channels has been commissioned, which has been developed specifically for STXM. A Fourier filtering reconstruction technique has been successfully implemented to reconstruct the complex specimen function from the partially coherent images recorded by the segments of the detector. The visualization of the phase shift becomes very important at higher photon energies and we plan to demonstrate phase contrast STXM at multi-keV energies using the segmented detector.

References

- [1] H. N. Chapman. Phase-retrieval x-ray microscopy by Wigner-distribution deconvolution. *Ultramicroscopy*, 66:153–172, 1996.
- [2] M. Feser. *Scanning transmission x-ray microscopy with a segmented detector*. PhD thesis, Department of Physics and Astronomy, Stony Brook University, 2002.
- [3] M. Feser, C. Jacobsen, P. Rehak, and G. DeGeronimo. Integrating silicon detector with segmentation for scanning transmission x-ray microscopy. in preparation.
- [4] B. L. Henke, E. M. Gullikson, and J. C. Davis. X-ray interactions: Photoabsorption, scattering, transmission, and reflection at $E=50\text{--}30,000$ eV, $Z=1\text{--}92$. *Atom. Data Nucl. Data*, 54:181–342, 1993.
- [5] J Kemmer. Fabrication of low noise silicon radiation detectors by the planar process. *Nucl. Instrum. Methods*, 169:499–502, 1980.
- [6] M.N. Landauer, B.C. McCallum, and J.M. Rodenburg. Double resolution imaging of weak phase specimens with quadrant detectors in the STEM. *Optik*, 100(1):37–46, 1995.

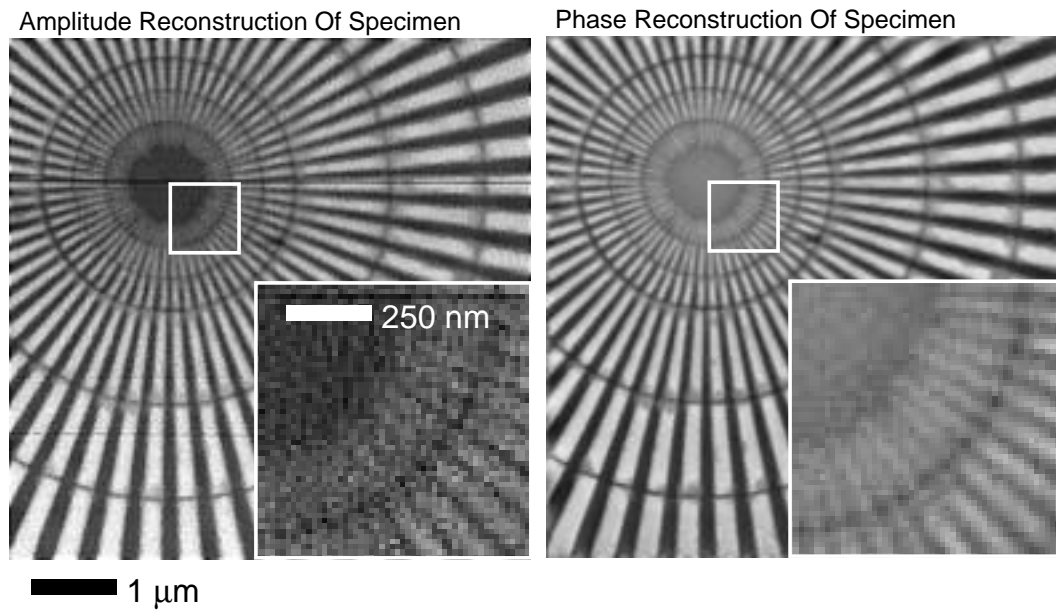


Fig. 4. Reconstructed images of the real and imaginary part of a Germanium test pattern.

- [7] B.C. McCallum, M.N. Landauer, and J.M. Rodenburg. Complex image reconstruction of weak specimens from a three-sector detector in the STEM. *Optik*, 101(2):53–62, 1995.
- [8] G. R. Morrison. STXM imaging with a configured detector. this proceedings.
- [9] J. R. Palmer and G. R. Morrison. Differential phase contrast imaging in the scanning transmission x-ray microscope. In P. H. Bucksbaum and N. M. Ceglio, editors, *OSA Proceedings on Short Wavelength Coherent Radiation: Generation and Applications*, volume 11, pages 141–145, Washington, D. C., 1991. Optical Society of America.
- [10] G. Schneider. Cryo x-ray microscopy with high spatial resolution in amplitude and phase contrast. *Ultramicroscopy*, 75:85–104, 1998.